A New Behavioral Paradigm for Studying Frustrative Non-reward in Juvenile Mice

Aijaz Ahmad Naik[1,2], Maxime Munyeshyaka [1], Xiaoyu Ma[1], Ellen Leibenluft[3], Zheng Li[1,*]

[1]Section on Synapse Development Plasticity, National Institute of Mental Health, National Institutes of Health, Bethesda, Maryland 20892

[2]Center on Compulsive Behaviors, Intramural Research program, NIH, Bethesda, MD, USA

[3]Section on Mood Dysregulation and Neuroscience, National Institute of Mental Health, National Institutes of Health, Bethesda, Maryland 20892

*Correspondence to Zheng Li
email: lizheng2mail@nih.gov; phone: 301-594-2269

Abstract

Background

Irritability, which can be defined as proneness to anger that can reach a pathological extent, is one of the most common reasons youth present for psychiatric evaluation and care. Aberrant responses to frustrative non-reward (FNR, the response to omission of an expected reward) are central to the pathophysiology of irritability. FNR is a cross-species RDoC construct. The development of preclinical FNR models could advance mechanistic studies of the important, and relatively understudied, clinical phenomenon of irritability.

Methods

We used FNR, a translational construct across species, as a conceptual framework for a novel behavioral paradigm (Alternate Poking Reward Omission, APRO) in mice. After APRO, mice were examined with a battery of behavioral tests to determine the effects of

frustration. Also, whole brain imaging of c-Fos expression was used to identify brain regions activated by FNR.

Results

Mice, regardless of sex, increased locomotion, and aggression towards conspecifics after APRO. There was no change in anxiety-like, depression-like, or non-aggressive social behaviors. APRO causes activation of 13 regions in the prelimbic, ACC, hippocampus, dorsal thalamus, cuneiform nucleus, pons, and pallidum areas, and shifts the brain network towards a more global processing mode.

Conclusion

Our novel FNR paradigm produces a frustration effect and alters brain processing in ways resembling the symptoms and brain network reconfiguration observed in youth with severe irritability. The novel behavioral paradigm and brain regions identified to be selectively activated by it lay the groundwork for further mechanistic studies of frustration and irritability in rodents.

Introduction:

Irritability, defined as proneness to anger that can reach a pathological extent, is one of the most common reasons for psychiatric evaluation and treatment in youth (1). It is associated with significant impairment and long-lasting adverse outcomes including high rates of school suspensions, hospitalizations, suicidality, and diagnoses of anxiety and depression (2, 3) . Irritability is the hallmark symptom of Disruptive Mood Dysregulation Disorder (DMDD), a disorder introduced into the Diagnostic and Statistical Manual of Mental Disorders (DSM-5). Current treatments for irritability are limited and not specific (4). Increased understanding of its neurobiological mechanisms would facilitate the development of novel, specific interventions. However, despite increased irritability research over the past decade, the neuroscience of irritability is still in its infancy (5-8). Progress has been slow partly due to the lack of behavioral paradigms for studying irritability in model organisms.

Studies suggest that youth with severe irritability have elevated responses to frustrative non-reward (FNR) i.e., the emotional and behavioral response to the omission of an expected reward (9). FNR is a translational, cross-species construct that can be leveraged to uncover pathophysiological mechanisms of irritability. The American psychologist Abram Amsel, a pioneer in the study of FNR, proposed that instrumental behavior is learned through frustrating, rewarding, and punishing events (10-13). However, in contrast to the much-studied rewarding and punishing events, little research has focused on the neural substrates of FNR. Amsel studied the effect of FNR on behavior using a double-runway setup in which rats were trained to walk through two runways connected in series to receive rewards at the end of each runway. After the rats learned

the task, FNR was introduced by reward omission (10, 13) . Amsel demonstrated that FNR invigorates behavior as indicated by faster running and increased resistance to extinction.

Besides the double-runway paradigm, an operant conditioning chamber has also been used to produce frustration in rodents. This method works better for adult animals with well-developed muscles than for juveniles because animals must learn to press a lever repeatedly to receive reward. Both the double-runway and operant conditioning chamber methods, however, require weeks of training (14-16). Long training periods are unsuited to study irritability-like behavior in mice, as DMDD is a disorder diagnosed in children aged 6–18, which corresponds to only 3–6 weeks of ages in mice (17). The short developmental period of mice restrains the duration of the behavioral paradigm.

Human studies of brain-based mechanisms of irritability are limited and have yielded mixed results (18). Preliminary studies find that high levels of irritability following frustration in patients with DMDD correspond with increased frontal-striatal activation in the anterior cingulate cortex, dorsolateral prefrontal cortex, caudate, amygdala, and parietal cortex (9, 19, 20). Recent network-based pilot studies using both task-based and resting-state fMRI found predictive associations between irritability and post-frustration connectivity in limbic, reward, and sensorimotor networks (9, 21). However, human fMRI studies with inadequate spatial and temporal resolution cannot identify the impact of frustration at the level of neuronal ensembles. The capacity to do so in animals would be a significant translational advance that could eventually lead to more precisely tailored innovative treatments for irritability and DMDD.

To study FNR in young mice, we developed a new behavioral paradigm named Alternate Poking Reward Omission (APRO). We show that after exposure to APRO, mice increase locomotion, aggression, and resistance to extinction of instrumental behavior. Whole-brain mapping of activated neurons identifies brain regions that are responsive to FNR and shows that the brain network is shifted to a more global processing mode by FNR.

Materials and Methods

Alternate poking reward omission (APRO)

Mice (35 days old; male and female) were placed under water restriction for three days during which they were given ad libitum access to water for 1 hour per day. The apparatus used for APRO was constructed by NIMH Section on Instrumentation. It is a closed running track (50L x 10W x 15H cm) with a spout installed at each end and a LED light mounted next to the spout. The mouse was allowed to run freely in the track for one 15-min session per day. The mouse could poke the port when it reached the end of the track. If the mouse poked the port other than the previous one it had poked, the LED light came on for 2 sec and a water drop was delivered from the spout.

During training sessions, the mouse received water reward for every correct port poking. Only mice making ≥12 licks on each side by Day 3 proceeded to Day 4 and 5 of APRO. On Days 4 and 5, mice run on the same track with the same rules. While control mice received water reward for all correct pokings on Days 4 and 5, water reward was delivered for only 50% of correct pokings on Day 4 and 20% on Day 5 for mice subjected to FNR. Thirty minutes after the FNR session on Day 5, the mice were subjected to a battery of behavioral tests, including the open field, resident intruder, elevated zero-maze,

light/dark, forced swim, sucrose preference, and three-chamber social preference tests. Different cohorts of mice were used for each behavioral test so that each mouse was subjected to only one behavioral test. For the extinction experiment performed on Day 6, mice were run in the track for 15 minutes without light or water reward regardless of which port they poked. All behavioral tests were conducted under red lights in the dark cycle of the animal. Behavioral data were analyzed blindly. More on Materials and Methods has been included in supplemental information.

Results

A new behavioral paradigm based on the frustrative non-reward framework

To study FNR, we designed a reward-seeking task that a mouse can learn within three days. We named this behavioral paradigm “alternate poking reward omission” (APRO). APRO, conducted in a linear track, has two stages which were completed in 5 days (Figure 1A, B). The rate of correct port poking increased over the training period and reached 100% on day 3 (Figure 1C, Table S1). For mice exposed to FNR (FNR mice), frustration was then induced by withholding reward 50% of the time on Day 4 and 80% of the time on Day 5.

FNR mice increased the number of visits to the ports on Days 4 and 5 (Figure 1D, Table S1). Additionally, FNR mice ran faster during the test session than control mice on Day 5 (Figure 1E, Table S1). When testing extinction on Day 6, FNR mice made more visits to the ports than control mice (Figure 1F, Table S1), indicating increased resistance to extinction.

Taken together, the FNR mice's behaviors in the APRO paradigm are consistent with Amsel's proposition that frustration increases running speed and resistance to the extinction of instrumental behavior.

FNR increases locomotion

We assessed the effect of FNR by conducting additional behavioral tests. Frustration is conceptualized as an adaptive motivational state that elevates activity and aggression (22-27). We, therefore, examined locomotion with the open field test (Figure 2A). Mice were tested within 30 min after the test session on Day 5. FNR mice traveled a longer distance in the arena during the open field test than control mice (Figure 2B, C; Table S1). However, the time spent in the center zone of the arena, which is an indicator of anxiety-like behavior, was comparable in control and FNR mice (Figure 2B, D; Table S1). Both male and female FNR mice exhibited hyperlocomotion (Figure 2B, C; Table S1).

The mice were under water restriction throughout APRO. Since control mice drank more water than FNR mice in the FNR session prior to the open field test, thirst may underlie the hyperlocomotion of FNR animals. To test the effect of thirst on locomotion, we conducted the open field test in mice who had been water restricted but not exposed to FNR. Water-restricted mice and control mice were comparable in the total distance travelled and time spent in the center zone (Figure 2B, C, D; Table S1). These results indicate that FNR, but not thirst, increases locomotion.

FNR increases aggression but not non-aggressive social interaction

Next, we examined the effect of FNR on aggression using a modified resident-intruder (RI) test in both control and FNR mice (Figure 3A). A FNR or control mouse (resident) was placed back in the home cage after the test session on Day 5 and allowed to freely explore the cage for 30 min. An unfamiliar, smaller mouse of the same sex (intruder) was then introduced into the same cage to interact with the resident mouse for 5 minutes (Figure 3A).

The control mice largely displayed non-aggressive social behaviors such as anogenital sniffing, grooming, and rearing towards the intruder. However, the FNR mice exhibited aggressive behaviors towards the intruder, such as clinch attack, keep down, lateral threat, and chasing (28-30). Compared to control mice, FNR mice had more total number of attacks, higher average attack duration per episode and total attack time, and a shorter latency to the first attack (Figure 3B-D, Table S1). Notably, C57BL/6 female mice, who usually are not aggressive in the RI test, also attacked the intruder after FNR (Figure 3B-D, Table S1). Water restriction alone had no effect on aggressive behavior (Figure 3B-D, Table S1). Non-aggressive social behavior during the RI test were comparable in FNR and control mice (Figure 3E, Table S1).

We further assessed the effect of FNR on social behavior using the three-chamber sociability test (31) (Figure 4A). FNR and control mice spent similar amounts of time exploring the conspecific and object (Figure 4B, C; Table S1), indicating comparable sociability. Males and females were pooled in data analysis as no sex differences were detected (Table S2). Taken together, these findings indicate that FNR elevates aggression in both male and female mice, without altering non-aggressive social interaction or sociability.

FNR has no effect on anxiety-like or depression-like behaviors

To test whether FNR impacts on anxiety-like behavior, we conducted the light/dark box and elevated zero-maze tests after the test session on Day 5 (Figure 5A). Each test used a different cohort of animals. In the elevated zero-maze test, the time spent in the open arms and the total number of entries into the open arms were comparable in control and FNR mice (Figure 5B, C; Table S1). Similarly, in the light-dark box test, the time spent in the light box and the total number of entries into the light box were comparable between control and FNR mice (Figure 5D, E; Table S1). Males and females were pooled in data analysis as no sex differences were detected (Table S2). These results indicate that FNR has no effect on anxiety-like behavior.

For depression-like behavior, we used the forced swim and sucrose preference tests to assess behavioral despair and anhedonia-like behavior. In the forced swim test, total immobility time and total number of immobile episodes were comparable in control and FNR mice (Figure 5F, G; Table S1). In the sucrose preference test, the ratio of sucrose to water consumed during after and 6 hr and 22 hr before the FNR session was comparable in control and FNR mice (Figure 5H, Table S1, S2). Males and females were pooled in data analysis as no sex differences were detected (Table S2).

These results indicate that FNR has no effect on anxiety-like or depression-like behaviors.

Brain-wide mapping of the effect of FNR on neural activity

To investigate the effect of FNR on brain activity, we removed the brains from the mice (4 control and 5 FNR) 90 minutes after the test session on Day 5 to label activated

neurons expressing c-Fos (Figure S1). The total number of c-Fos positive cells was greater in the FNR than control brains ($1.24 \pm 0.13 \times 10^6$ for control and $1.95 \pm 0.13 \times 10^6$ for FNR; $p = 0.001$, two-tailed Student's t-test). We parcellated the whole brain according to the Allen Mouse Brain Common Coordinate Framework and removed regions with only a few c-Fos positive cells from the list for further analysis as the signal-to-noise ratio was relatively low and the variability between animals was relatively large.

Of the 87 brain regions that we analyzed, 13 regions including prelimbic area, dorsal and ventral parts of the anterior cingulate area, pretectal region, CA2, anterior group of dorsal thalamus, geniculate and medial groups of the dorsal thalamus, cuneiform nucleus, intralaminar nuclei of dorsal thalamus, frontal pole, pons (behavioral state related), and medial region of pallidum showed statistically significant differences between FNR and control mice (two-tailed Student's t-test corrected for FDR with Benjamini–Hochberg procedure, $p < 0.05$; Figure 6; Table S3).

To interrogate the brain response to FNR at a brain-wide level, we constructed correlation matrices for the control and FNR groups (Figure 7A, B). The correlation matrices showed that brain regions within the same anatomical divisions were not always co-activated. Then, based on the correlation matrices, we examined how well the brain network can be subdivided into non-overlapping modules by computing the modularity index Q for each group. The FNR brain had lower Q at all network intensities (Figure 7C), suggestive of a more global processing mode than the control brain.

To compare modular structures between the FNR and control brains, we performed hierarchical consensus clustering analysis (HCC) to build a hierarchy of clusters with

increasingly strong interregional correlations (32). HCC revealed a nested community structure with up to 5 levels and 7 modules in the control group, and 6 levels and 7 modules in FNR group. While some brain regions in the same HCC cluster belonged to the same anatomical division, HCC clusters were distinct from the anatomical grouping of brain regions (Figure 7, 8). The cluster composition was different between control and FNR brains (Figure 9), suggestive of a reconfiguration of brain network by FNR. For example, 8 of the 13 brain regions with more c-Fos positive cells in FNR brains were distributed across multiple modules in control brains but clustered in the same module in FNR brains (Figure 9).

Discussion

Irritability is among the most common reasons that children are brought for psychiatric evaluation and care (1, 2, 6, 33, 34). Despite the significant impact of irritability on mental health, little is known about its underlying neural mechanisms and limited treatment options are available (4, 35). Mechanistic understanding of irritability is needed to guide development of new treatments. Youths with severe irritability have elevated responses to FNR; the latter is a cross-species, translational construct (9, 35, 36). Therefore, translational research elucidating the neurobiology of FNR can facilitate research on the pathophysiology of irritability. Consistent with this, FNR is a construct in the negative valance system in Research Domain Criteria (RDoC) (36). Importantly, even though Amsel's frustration theory has been examined extensively from a behavioral perspective since the 1950s, few studies attempt to disentangle the underlying brain circuits and neural mechanisms.

To that end, we developed a mouse behavioral paradigm (APRO) based on FNR to study irritability-like behavior in juvenile mice. This paradigm takes advantage of the mouse's natural tendency of alternating visits between two places to complete training within 3 days, significantly shorter than older paradigms e.g., double runway and operant conditioning methods (14-16). We demonstrated that following APRO, FNR mice increased locomotion, aggression, and resistance to extinction of learned behavior. These behavioral alterations are consistent with frustration effects reported in rats, chimpanzees, pigeons, and humans (10, 11, 13, 22-24, 26, 37-41). However, our FNR mice had no change in anxiety-like or depression-like behavior, or social preference. This suggests that the effects of FNR are relatively specific, inducing behavioral changes that are directly relevant to those seen in youth with severe irritability who have frequent temper outbursts, characterized by increased motor activity and aggression (41, 42).

Functional magnetic resonance imaging (fMRI) based on blood-oxygenation−dependent signals (BOLD) has been used to study brain activity related to irritability in humans. However, the spatial resolution, signal to noise ratio, and incomplete understanding of the factors contributing to BOLD signals limit the precision and details of the derived brain activity map. Our whole-brain imaging of c-Fos labeling provides more refined and direct measurement of neural activity compared to fMRI studies. We elected to stain for c-Fos because it is a commonly used marker of cell activation (43-46) and its nuclear localization assists machine learning-based cell segmentation and automated cell counting.

13 brain regions including prelimbic area, dorsal and ventral parts of the anterior cingulate area, pretectal region, CA2, anterior group of dorsal thalamus, geniculate and medial groups of the dorsal thalamus, cuneiform nucleus, intralaminar nuclei of dorsal thalamus,

frontal pole, pons (behavioral state related), and medial region of pallidum showed significant changes to c-Fos in FNR, compared to control, mice. Some of these brain regions have been associated with negative emotions and high irritability, such as the hippocampus, thalamus, and ACC of the limbic system. ACC lesions in humans are associated with hostility, emotional unconcern, and irresponsibility (24, 47). Human neuroimaging studies show that emotional provocation enhances the activity of amygdala, hypothalamus, and PAG (48, 49). In addition to being a sensory relay center, the role of the anterior and midline group thalamic nuclei in response to aversive and rewarding stimuli has emerged from recent rodent studies (50-53). In addition to identifying candidate brain regions potentially involved in the behavioral responses to FNR, our analysis of brain activation networks found that FNR changes the modular composition of the brain, specifically reducing modularity and thereby creating a more global processing mode.

Although our APRO paradigm produces robust and specific behavioral changes in both male and female C57BL/6 mice, it has yet to be determined by future studies if APRO is applicable to other strains of mice and if so, what are the behavioral effects. It is possible that APRO produces strain specific behavioral changes given the genetic, physiological, and behavioral variations among mouse strains. If this is true, strain-dependent responses to APRO expand the capacity of using mice to study individual differences in FNR, research which would facilitate clinical research on individual differences in irritability. Applying APRO to mice predisposed to anxiety-like or depression-like behavior, such as mice harboring mutations in genes increasing risk for psychiatric disorders or

exposed to environmental risk factors, is another avenue of future research that could provide insights into the complex pathogenic mechanisms of human irritability.

c-Fos labeling is a robust method to generate a whole-brain activation map, which guides the formulation of hypotheses for further studies. As the animal is typically perfused ~90 min post stimulation to allow c-Fos proteins to accumulate to detectable levels (43), the temporal resolution of c-Fos reported brain activation is low. The fixation step also makes this method unsuitable for time-lapse imaging in the same subject. In addition, the specific type of neurons that are activated are unclear from measurement of endogenous c-Fos as it is ubiquitously expressed in all neurons. This limitation can be addressed in future studies using transgenic mice that express c-Fos promoter driven fluorescent proteins in a cell-type specific manner. Despite these limitations, our c-Fos study provides a detailed landscape of brain activity change in response to FNR, pinpointing specific brain regions that can be precisely manipulated and measured with advanced genetic, optogenetic, and electrophysiological tools to dissect the neural mechanism of FNR and irritability in future studies.

Conflicts of Interest

The authors have no conflicts or competing interests to disclose

Acknowledgements and Funding

This work was supported by the Intramural Research Program of the National Institute of Mental Health (ZIAMH002881 to Z.L. and ZIAMH002786 to E.L) and the Center on Compulsive Behaviors (CCB), NIH via the NIH Shared resource Subcommittee to A.N.

A.N. is a first year CCB-2022 fellow. We thank Dr. Ted Usdin (NIMH) for co-mentoring A.N. for the CCB fellowship program and summer student Jeffrey Zhang from Oberlin College and Conservatory for assistance in behavioral data analysis. We thank NIMH IRP Rodent Behavior core for support of behavioral analysis, LifeCanvas Technologies for assistance with c-Fos whole brain immunohistochemistry and light-sheet imaging.

References

1. Evans SC, Corteselli KA, Edelman A, Scott H, Weisz JR (2022): Is Irritability a Top Problem in Youth Mental Health Care? A Multi-informant, Multi-method Investigation. *Child Psychiatry Hum Dev*.

2. Leibenluft E (2017): Pediatric Irritability: A Systems Neuroscience Approach. *Trends Cogn Sci*. 21:277-289.

3. Copeland WE, Angold A, Costello EJ, Egger H (2013): Prevalence, comorbidity, and correlates of DSM-5 proposed disruptive mood dysregulation disorder. *Am J Psychiatry*. 170:173-179.

4. Breaux R, Baweja R, Eadeh HM, Shroff DM, Cash AR, Swanson CS, et al. (2022): Systematic Review and Meta-analysis: Pharmacological and Non-pharmacological Interventions for Persistent Non-episodic Irritability. *J Am Acad Child Adolesc Psychiatry*.

5. Damme KSF, Norton ES, Briggs-Gowan MJ, Wakschlag LS, Mittal VA (2022): Developmental patterning of irritability enhances prediction of psychopathology in preadolescence: Improving RDoC with developmental science. *J Psychopathol Clin Sci*. 131:556-566.

6. Leibenluft E, Stoddard J (2013): The developmental psychopathology of irritability. *Dev Psychopathol*. 25:1473-1487.

7. Stringaris A, Vidal-Ribas P, Brotman MA, Leibenluft E (2018): Practitioner Review: Definition, recognition, and treatment challenges of irritability in young people. *J Child Psychol Psychiatry*. 59:721-739.

8. Vidal-Ribas P, Brotman MA, Valdivieso I, Leibenluft E, Stringaris A (2016): The Status of Irritability in Psychiatry: A Conceptual and Quantitative Review. *J Am Acad Child Adolesc Psychiatry*. 55:556-570.

9. Linke JO, Haller SP, Xu EP, Nguyen LT, Chue AE, Botz-Zapp C, et al. (2022): Persistent Frustration-Induced Reconfigurations of Brain Networks Predict Individual Differences in Irritability. *J Am Acad Child Adolesc Psychiatry*.

10. Amsel A, Hancock W (1957): Motivational properties of frustration. III. Relation of frustration effect to antedating goal factors. *J Exp Psychol*. 53:126-131.

11. Abler B, Walter H, Erk S (2005): Neural correlates of frustration. *Neuroreport*. 16:669-672.

12. Kircanski K, Craske MG, Averbeck BB, Pine DS, Leibenluft E, Brotman MA (2019): Exposure therapy for pediatric irritability: Theory and potential mechanisms. *Behav Res Ther*. 118:141-149.

13. Amsel A (1958): The role of frustrative nonreward in noncontinuous reward situations. *Psychol Bull*. 55:102-119.

14. Burokas A, Gutierrez-Cuesta J, Martin-Garcia E, Maldonado R (2012): Operant model of frustrated expected reward in mice. *Addict Biol*. 17:770-782.

15. Staddon JE, Cerutti DT (2003): Operant conditioning. *Annu Rev Psychol*. 54:115-144.

16. Vasquez TES, Shah P, Re JD, Laezza F, Green TA (2021): Individual Differences in Frustrative Nonreward Behavior for Sucrose in Rats Predict Motivation for Fentanyl under Progressive Ratio. *eNeuro*. 8.

17. Dutta S, Sengupta P (2016): Men and mice: Relating their ages. *Life Sciences*. 152:244-248.

18. Lee KS, Hagan CN, Hughes M, Cotter G, McAdam Freud E, Kircanski K, et al. (2023): Systematic Review and Meta-analysis: Task-based fMRI Studies in Youths With Irritability. *J Am Acad Child Adolesc Psychiatry*. 62:208-229.

19. Scheinost D, Dadashkarimi J, Finn ES, Wambach CG, MacGillivray C, Roule AL, et al. (2021): Functional connectivity during frustration: a preliminary study of predictive modeling of irritability in youth. *Neuropsychopharmacology*. 46:1300-1306.

20. Tseng WL, Deveney CM, Stoddard J, Kircanski K, Frackman AE, Yi JY, et al. (2019): Brain Mechanisms of Attention Orienting Following Frustration: Associations With Irritability and Age in Youths. *Am J Psychiatry*. 176:67-76.

21. Naim R, Haller SP, Linke JO, Jaffe A, Stoddard J, Jones M, et al. (2022): Context-dependent amygdala-prefrontal connectivity during the dot-probe task varies by irritability and attention bias to angry faces. *Neuropsychopharmacology*. 47:2283-2291.

22. Azrin NH, Hutchinson RR, Hake DF (1966): Extinction-induced aggression. *J Exp Anal Behav*. 9:191-204.

23. Berkowitz L (1989): Frustration-aggression hypothesis: examination and reformulation. *Psychol Bull*. 106:59-73.

24. Bertsch K, Florange J, Herpertz SC (2020): Understanding Brain Mechanisms of Reactive Aggression. *Curr Psychiatry Rep*. 22:81.

25. Nelson RJ, Trainor BC (2007): Neural mechanisms of aggression. *Nat Rev Neurosci*. 8:536-546.

26. Yu R, Mobbs D, Seymour B, Rowe JB, Calder AJ (2014): The neural signature of escalating frustration in humans. *Cortex*. 54:165-178.

27. Deveney CM, Connolly ME, Haring CT, Bones BL, Reynolds RC, Kim P, et al. (2013): Neural mechanisms of frustration in chronically irritable children. *Am J Psychiatry*. 170:1186-1194.

28. Koolhaas JM, Coppens CM, de Boer SF, Buwalda B, Meerlo P, Timmermans PJ (2013): The resident-intruder paradigm: a standardized test for aggression, violence and social stress. *J Vis Exp*.e4367.

29. Lischinsky JE, Lin D (2020): Neural mechanisms of aggression across species. *Nat Neurosci*. 23:1317-1328.

30. Nordman J, Ma X, Li Z (2020): Traumatic Stress Induces Prolonged Aggression Increase through Synaptic Potentiation in the Medial Amygdala Circuits. *eNeuro*. 7.

31. Rein B, Ma K, Yan Z (2020): A standardized social preference protocol for measuring social deficits in mouse models of autism. *Nat Protoc*. 15:3464-3477.

32. Jeub LGS, Sporns O, Fortunato S (2018): Multiresolution Consensus Clustering in Networks. *Sci Rep*. 8:3259.

33. Perlman SB, Jones BM, Wakschlag LS, Axelson D, Birmaher B, Phillips ML (2015): Neural substrates of child irritability in typically developing and psychiatric populations. *Dev Cogn Neurosci*. 14:71-80.

34. Krieger FV, Leibenluft E, Stringaris A, Polanczyk GV (2013): Irritability in children and adolescents: past concepts, current debates, and future opportunities. *Braz J Psychiatry*. 35 Suppl 1:S32-39.

35. Eshel N, Leibenluft E (2020): New Frontiers in Irritability Research-From Cradle to Grave and Bench to Bedside. *JAMA Psychiatry*. 77:227-228.

36. Ametti MR, Crehan ET, O'Loughlin K, Schreck MC, Dube SL, Potter AS, et al. (2022): Frustration, Cognition, and Psychophysiology in Dysregulated Children: A Research Domain Criteria Approach. *J Am Acad Child Adolesc Psychiatry*. 61:796-808 e792.

37. Amsel A, Roussel J (1952): Motivational properties of frustration. I. Effect on a running response of the addition of frustration to the motivational complex. *J Exp Psychol*. 43:363-366.

38. Henna E, Zilberman ML, Gentil V, Gorenstein C (2008): Validity of a frustration-induction procedure. *Braz J Psychiatry*. 30:47-49.

39. Amsel A, Ward JS (1954): Motivational properties of frustration: II. Frustration drive stimulus and frustration reduction in selective learning. *J Exp Psychol*. 48:37-47.

40. Scott JP (1948): Dominance and the frustration-aggression hypothesis. *Physiol Zool*. 21:31-39.

41. Yu RJ (2016): The Neural Basis of Frustration State. *Neuroimaging Personality, Social Cognition and Character*.223-243.

42. Brotman MA, Kircanski K, Stringaris A, Pine DS, Leibenluft E (2017): Irritability in Youths: A Translational Model. *Am J Psychiatry*. 174:520-532.

43. Morgan JI, Cohen DR, Hempstead JL, Curran T (1987): Mapping patterns of c-fos expression in the central nervous system after seizure. *Science*. 237:192-197.

44. Sheng M, Greenberg ME (1990): The regulation and function of c-fos and other immediate early genes in the nervous system. *Neuron*. 4:477-485.

45. Naik AA, Brodovskaya A, Subedi S, Akram A, Kapur J (2022): Extrahippocampal seizure and memory circuits overlap. *eNeuro*. 9.

46. Naik AA, Sun H, Williams CL, Weller DS, Julius Zhu J, Kapur J (2021): Mechanism of seizure-induced retrograde amnesia. *Prog Neurobiol*. 200:101984.

47. Repple J, Pawliczek CM, Voss B, Siegel S, Schneider F, Kohn N, et al. (2017): From provocation to aggression: the neural network. *BMC Neurosci*. 18:73.

48. Mobbs D, Marchant JL, Hassabis D, Seymour B, Tan G, Gray M, et al. (2009): From threat to fear: the neural organization of defensive fear systems in humans. *J Neurosci*. 29:12236-12243.

49. Mobbs D, Petrovic P, Marchant JL, Hassabis D, Weiskopf N, Seymour B, et al. (2007): When fear is near: threat imminence elicits prefrontal-periaqueductal gray shifts in humans. *Science*. 317:1079-1083.

50. Otis JM, Zhu M, Namboodiri VMK, Cook CA, Kosyk O, Matan AM, et al. (2019): Paraventricular Thalamus Projection Neurons Integrate Cortical and Hypothalamic Signals for Cue-Reward Processing. *Neuron*. 103:423-431 e424.

51. Alcaraz F, Naneix F, Desfosses E, Marchand AR, Wolff M, Coutureau E (2016): Dissociable effects of anterior and mediodorsal thalamic lesions on spatial goal-directed behavior. *Brain Struct Funct*. 221:79-89.

52. Sweeney-Reed CM, Buentjen L, Voges J, Schmitt FC, Zaehle T, Kam JWY, et al. (2021): The role of the anterior nuclei of the thalamus in human memory processing. *Neurosci Biobehav Rev*. 126:146-158.

53. Roy DS ZY, Halassa MM, Feng G. (2022): Thalamic subnetworks as units of function. *Nat Neurosci*.13.

Figure legends

Figure 1. A novel frustrative non-reward paradigm applicable to juvenile mice. (A) Schematic of the experimental paradigm showing the two stages of APRO that begins at P35: training (Days 1-3) and reward omission (FNR; Day 4 & 5). An extinction protocol was applied on Day 6 to test the FNR effect. (B) Schematic drawing of the closed track apparatus installed with infrared-based sensors for poke-triggered cue light and reward delivery system. (C) The percentage of successful alternations between two ports across the three trainings days. (D) The number of port visits in the closed track across days. (E) The average instantaneous running speed between ports on Day 5. (F) The number of port visits during extinction on Day 6. Data are presented as mean + SEM; the numbers in the bars represent the number of animals; * $p < 0.05$, ** $p < 0.01$, *** $p < 0.001$.

Figure 2. FNR induces hyperlocomotion in both male and female mice. (A) Experimental schedule of APRO followed by open field test and Illustration of division of the central and peripheral zones; the cyan and red lines indicate the mouse's trajectory in the testing arena. (B) Representative mobility heatmaps showing the activity of male and female mice from different groups within the open field arena. (C) Total distance travelled by control, water restricted, and frustrated mice grouped by sex in a 20-minute testing session. (D) Total time spent in the central zone (25% of the testing arena) by male and female mice of different groups. FNR: frustrative non-reward; WR: water-restricted only; Con: control. Data are presented as mean + SEM; the numbers in the bars represent the number of animals; * $p < 0.05$.

Figure 3. FNR increases aggressive behavior in both male and female mice. (A) Experimental schedule of APRO followed by the resident intruder test. (B) The latency to the first attack in male and female mice. (C) The total time the resident mouse spent attacking the intruder. (D) The number of attack events during the resident-intruder test. (E) The total time spent in non-aggressive social interaction. Data are presented as mean + SEM; the numbers in the bars represent the number of animals; * $p < 0.05$, ** $p < 0.01$, *** $p < 0.001$.

Figure 4. FNR has no effect on social preference. (A) Experimental schedule of APRO followed by the three-chamber social preference test. (B) Representative heat maps showing the activity of the mouse in the mouse and object zone along with the neutral zone. (C)The total time spent with social stimulus (another mouse) and non-social stimulus (object) during the test by control and FNR groups. Data are presented as mean + SEM; N =16 for each group; *** $p < 0.001$.

Figure 5. **FNR has no effect on anxiety-like or depression-like behaviors.** (A) Schematic drawing of the experimental schedule. The elevated zero-maze (EZM), light/dark box test, forced swim test (FST), and sucrose preference test (SPT) followed APRO; different cohorts of mice were used for each test. (B) Total entries of the open arms in the EZM test. (C) Total time spent in the open arms during the EZM test. (D) Total entries of the light box in the light/dark box test. (F) Total time spent in the light box during the light/dark box test. (G) Total time mouse was immobile during FST. (H) The number of immobile events during FST. (H) shows the ratio of sucrose consumption over water recorded 6 and 22 hours after the Day 5 test session in control and FNR group mice. Data are presented as mean + SEM; the numbers in the bars represent the number of animals.

Figure 6. APRO induces brain activation. Control and FNR brains were stained for c-Fos after APRO on Day 5. (A) Heatmaps of the average c-FOS$^+$ cell density for the control (n = 4 brains) and FNR (n = 5 brains) groups at different bregma levels. Darker colors indicate higher density of c-FOS$^+$ cells. (B) Histograms showing the quantification of c-FOS$^+$ cells (cells/mm^3) in the 87 brain regions; data are presented as mean + SEM; *p<0.05; **p<0.01.

Figure 7. Brain networks of co-activation in control and FNR animals. (A, B) Inter-brain region correlation matrices for control (A) and FNR mice (B). Regions are sorted by anatomical division according to the Allen Brain Atlas. Colored dots at the top and left of the graph represent the anatomical division that each region belongs to. (C) Modularity index across network density thresholding. * p < 0.05.

Figure 8. Hierarchical consensus clustering of brain regions by co-activation. Hierarchical consensus clustering of the brain regions for control (A) and FNR mice (B). Regions enclosed by green boxes are highly correlated regions (α < 0.001) The dendrogram to the right of the matrices show the nested modular structures. Colored dots at the top of the matrices represent the anatomical division that each region belongs to.

Figure 9. The modular structures of control and FNR brains are different. The same brain regions are connected by lines between the hierarchical consensus clustering dendrograms for control (left) and FNR (right) brains. Brain regions within the same cluster of the control brain are indicated with the same color and the same color scheme applied to both control and FNR brains. Red arrows point to the brain regions that show significant differences in c-Fos density between control and FNR mice.

Fig. S1. Representative c-Fos images and registration to Allen Brain Atlas. The brains were processed for c-Fos staining after APRO and imaged with light-sheet microscopy. (A) Representative image taken at the level of the medial prefrontal cortex. (B) The image in A was registered with the Allen Brain Atlas and the 87 brain regions localized in this image were labeled. (C) Representative image containing the hippocampus. (D) The image in C was registered with the Allen Brain Atlas and the 87 brain regions localized in this image were labeled.

Figure 1

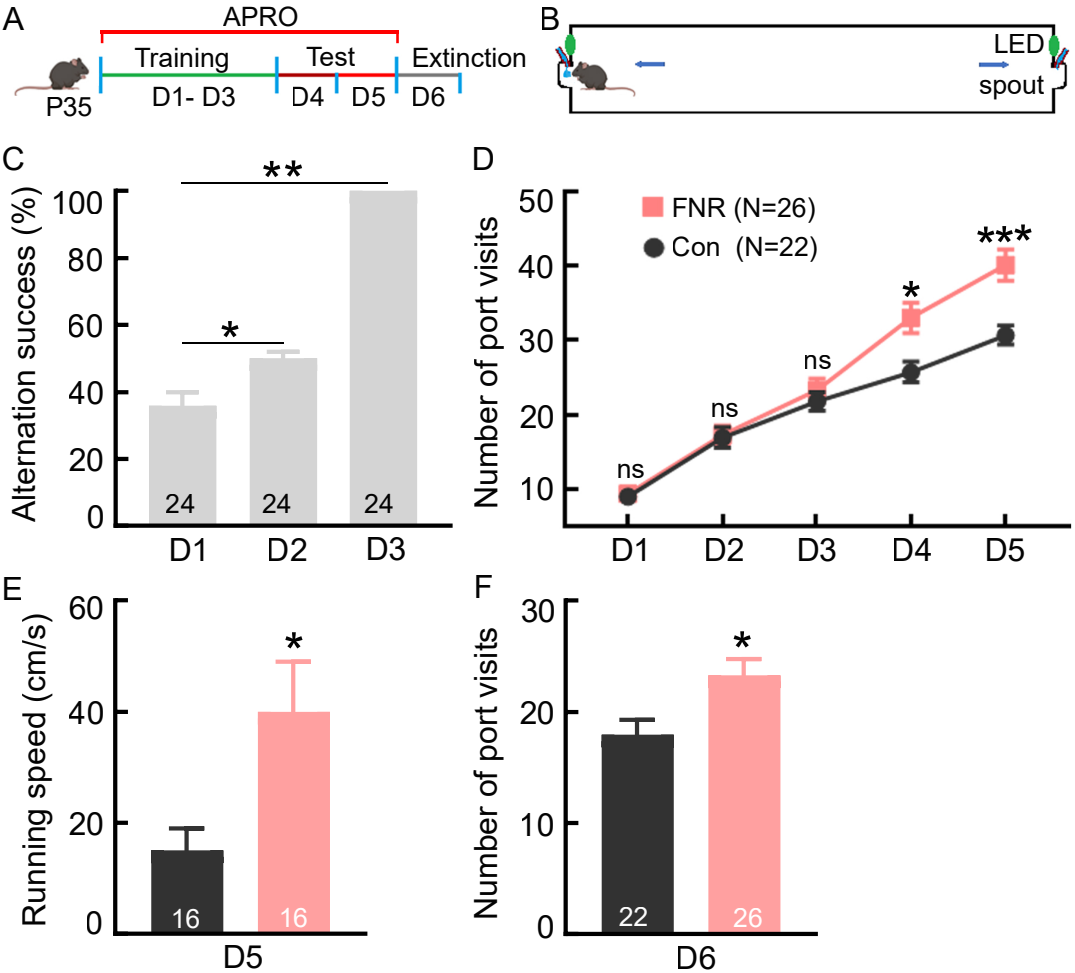
A
APRO
Training
Test
Extinction
P35
D1- D3
D4
D5
D6
B
LED
spout
C
Alternation success (%)
100
80
60
40
20
0
**
*
24
24
24
D1
D2
D3
D
Number of port visits
50
40
30
20
10
FNR (N=26)
Con (N=22)
***
*
ns
ns
ns
D1
D2
D3
D4
D5
E
Running speed (cm/s)
60
40
20
0
*
16
16
D5
F
Number of port visits
30
20
10
0
*
22
26
D6

Figure 2

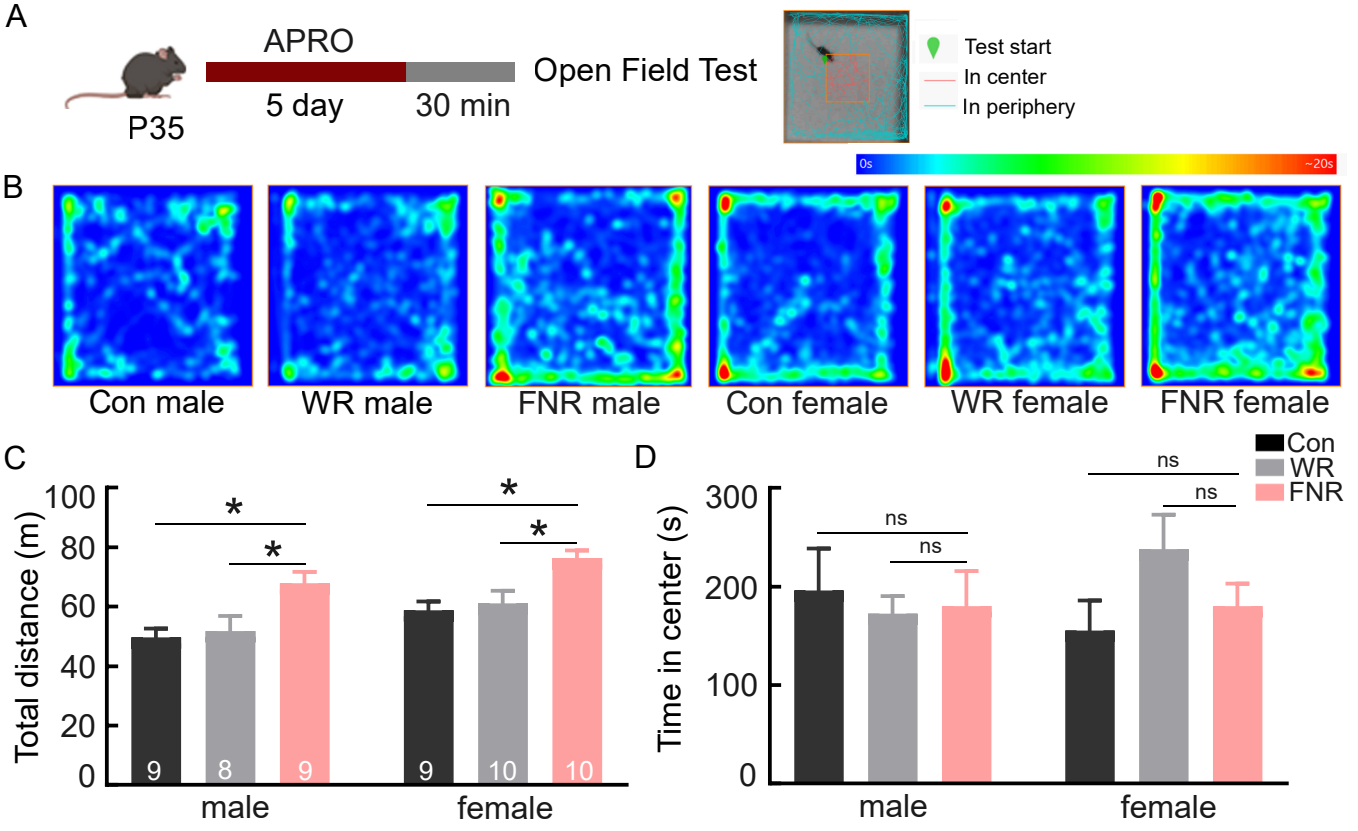
A
APRO
P35
5 day
30 min
Open Field Test
Test start
In center
In periphery
0s
~20s
B
Con male
WR male
FNR male
Con female
WR female
FNR female
C
Total distance (m)
100
80
60
40
20
0
*
*
*
*
9
8
9
9
10
10
male
female
D
Time in center (s)
300
200
100
0
ns
ns
ns
ns
male
female
Con
WR
FNR

Figure 3

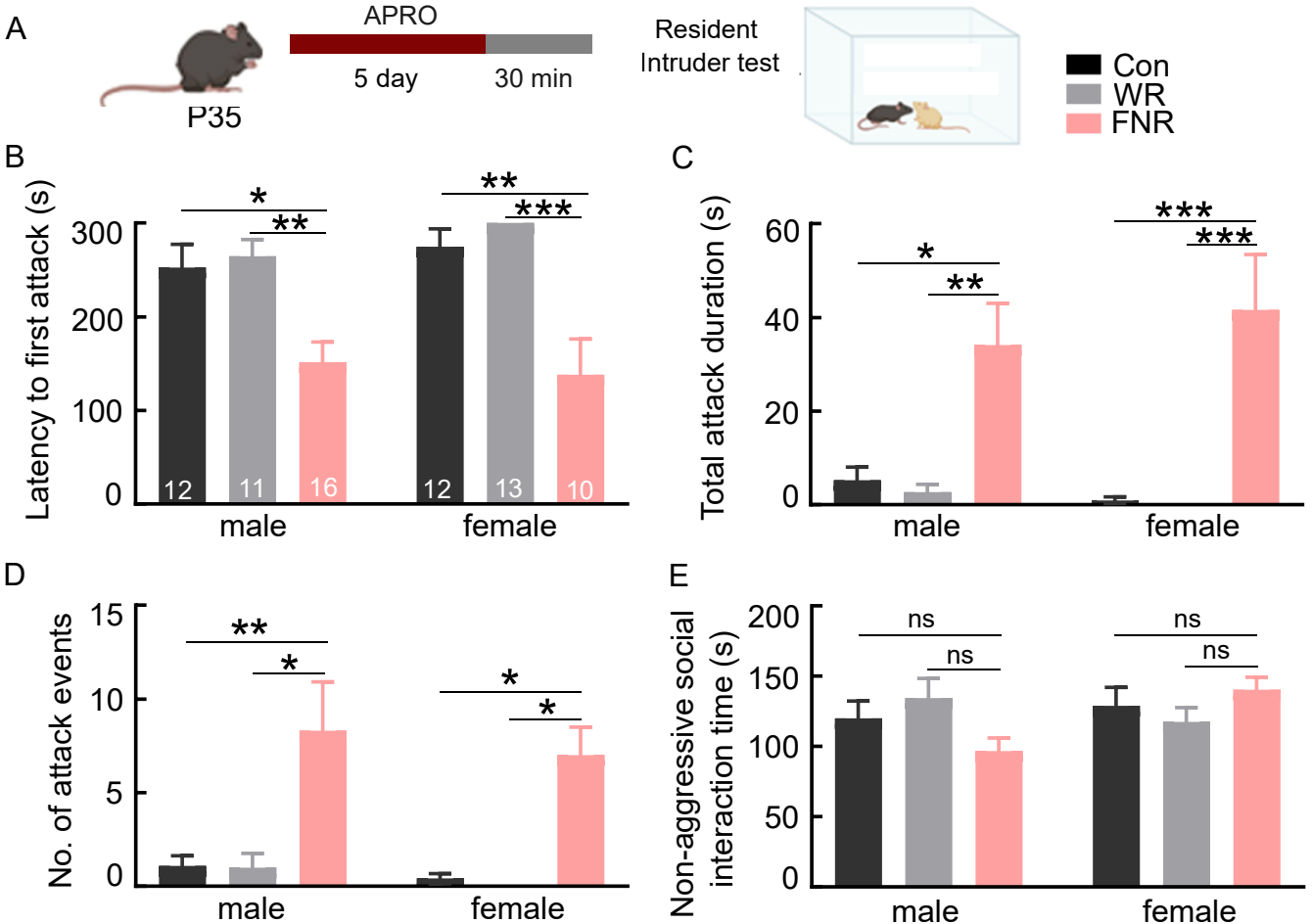
A
APRO
5 day
30 min
P35
Resident
Intruder test
Con
WR
FNR
B
Latency to first attack (s)
300
200
100
0
12
11
16
12
13
10
male
female
C
Total attack duration (s)
60
40
20
0
male
female
D
No. of attack events
15
10
5
0
male
female
E
Non-aggressive social interaction time (s)
200
150
100
50
0
ns
male
female

Figure 4

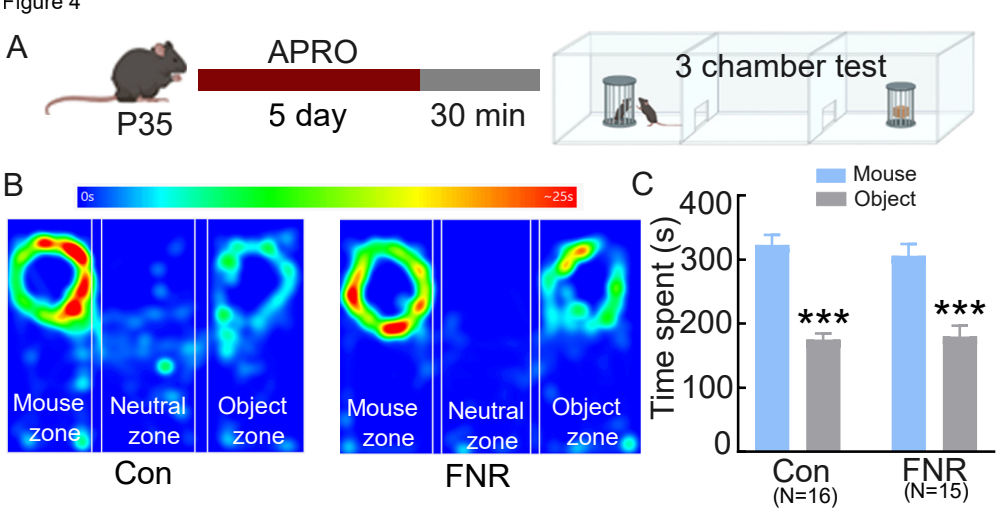
A
P35
APRO
5 day
30 min
3 chamber test
B
0s
~25s
Mouse zone
Neutral zone
Object zone
Con
FNR
C
Mouse
Object
Time spent (s)
400
300
200
100
0
***
***
Con
(N=16)
FNR
(N=15)

Figure 5

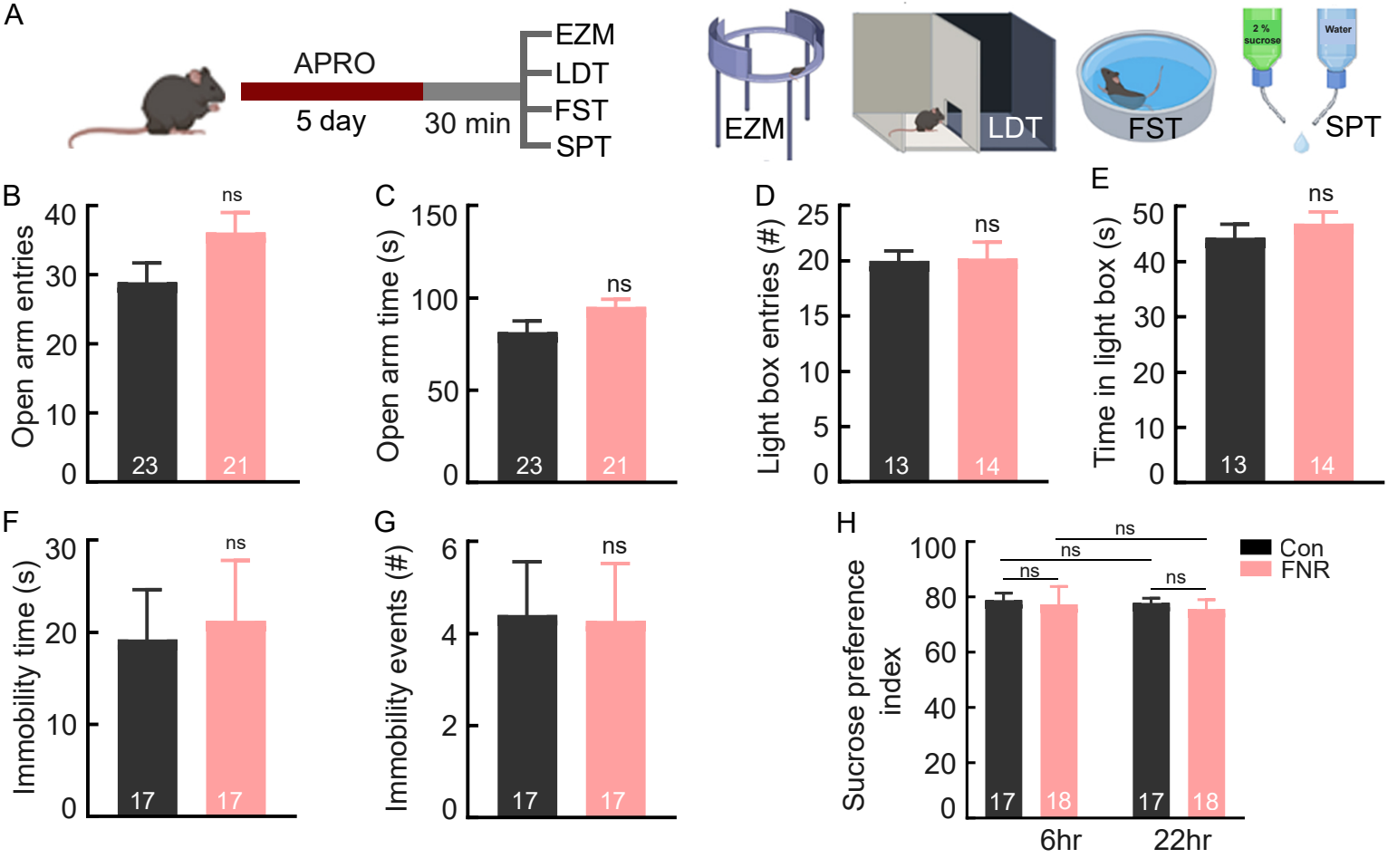
A
APRO
5 day
30 min
EZM
LDT
FST
SPT
EZM
LDT
FST
2 % sucrose
Water
SPT
B
Open arm entries
ns
23
21
C
Open arm time (s)
ns
23
21
D
Light box entries (#)
ns
13
14
E
Time in light box (s)
ns
13
14
F
Immobility time (s)
ns
17
17
G
Immobility events (#)
ns
17
17
H
Sucrose preference index
ns
ns
ns
ns
Con
FNR
17
18
17
18
6hr
22hr

Figure 6

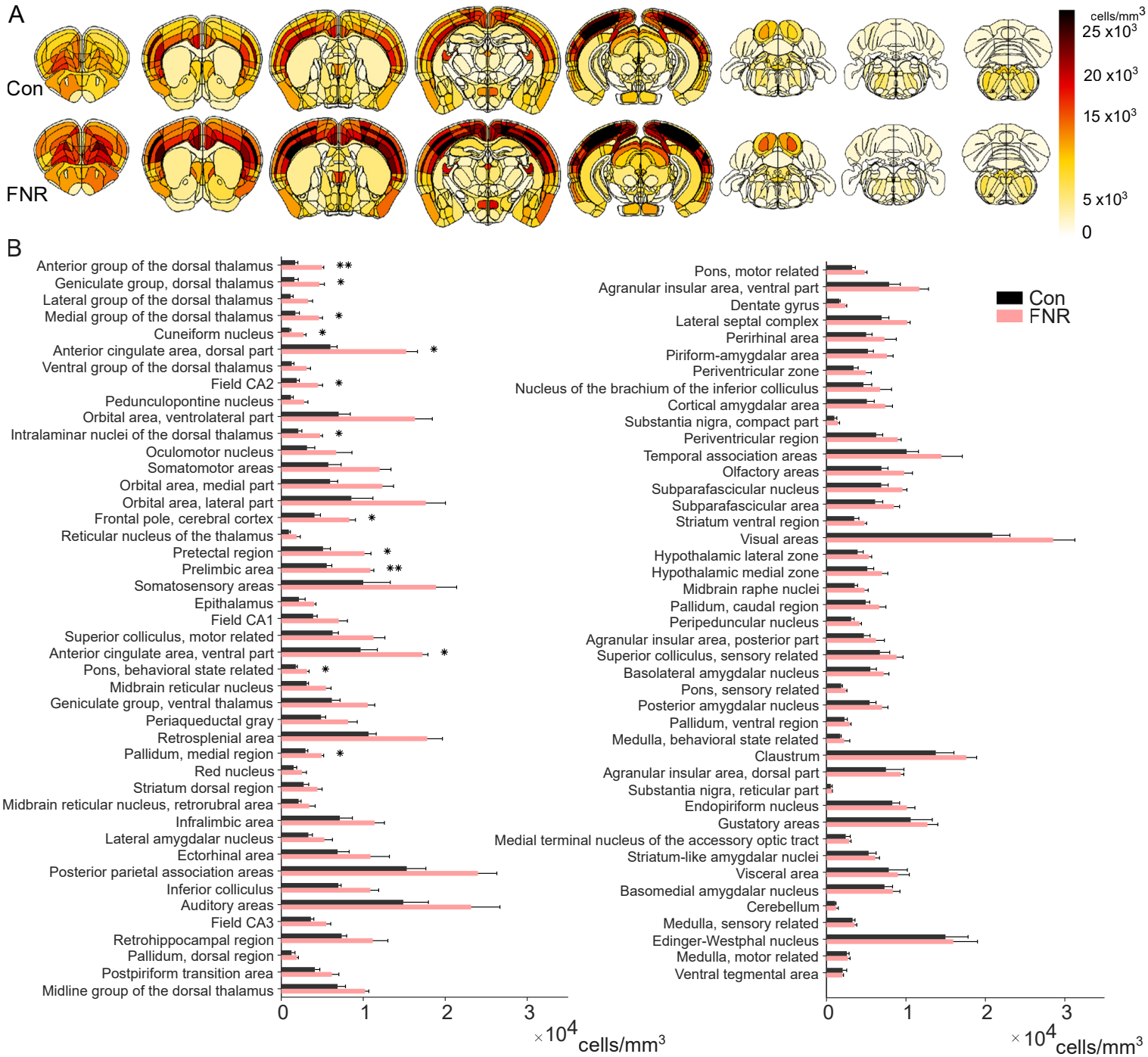
A
Con
FNR
cells/mm3
25 x10^3
20 x10^3
15 x10^3
5 x10^3
0
B
Anterior group of the dorsal thalamus
Geniculate group, dorsal thalamus
Lateral group of the dorsal thalamus
Medial group of the dorsal thalamus
Cuneiform nucleus
Anterior cingulate area, dorsal part
Ventral group of the dorsal thalamus
Field CA2
Pedunculopontine nucleus
Orbital area, ventrolateral part
Intralaminar nuclei of the dorsal thalamus
Oculomotor nucleus
Somatomotor areas
Orbital area, medial part
Orbital area, lateral part
Frontal pole, cerebral cortex
Reticular nucleus of the thalamus
Pretectal region
Prelimbic area
Somatosensory areas
Epithalamus
Field CA1
Superior colliculus, motor related
Anterior cingulate area, ventral part
Pons, behavioral state related
Midbrain reticular nucleus
Geniculate group, ventral thalamus
Periaqueductal gray
Retrosplenial area
Pallidum, medial region
Red nucleus
Striatum dorsal region
Midbrain reticular nucleus, retrorubral area
Infralimbic area
Lateral amygdalar nucleus
Ectorhinal area
Posterior parietal association areas
Inferior colliculus
Auditory areas
Field CA3
Retrohippocampal region
Pallidum, dorsal region
Postpiriform transition area
Midline group of the dorsal thalamus
0
1
2
3
×10^4 cells/mm3
Pons, motor related
Agranular insular area, ventral part
Dentate gyrus
Lateral septal complex
Perirhinal area
Piriform-amygdalar area
Periventricular zone
Nucleus of the brachium of the inferior colliculus
Cortical amygdalar area
Substantia nigra, compact part
Periventricular region
Temporal association areas
Olfactory areas
Subparafascicular nucleus
Subparafascicular area
Striatum ventral region
Visual areas
Hypothalamic lateral zone
Hypothalamic medial zone
Midbrain raphe nuclei
Pallidum, caudal region
Peripeduncular nucleus
Agranular insular area, posterior part
Superior colliculus, sensory related
Basolateral amygdalar nucleus
Pons, sensory related
Posterior amygdalar nucleus
Pallidum, ventral region
Medulla, behavioral state related
Claustrum
Agranular insular area, dorsal part
Substantia nigra, reticular part
Endopiriform nucleus
Gustatory areas
Medial terminal nucleus of the accessory optic tract
Striatum-like amygdalar nuclei
Visceral area
Basomedial amygdalar nucleus
Cerebellum
Medulla, sensory related
Edinger-Westphal nucleus
Medulla, motor related
Ventral tegmental area
Con
FNR
0
1
2
3
×10^4 cells/mm3

Figure 7

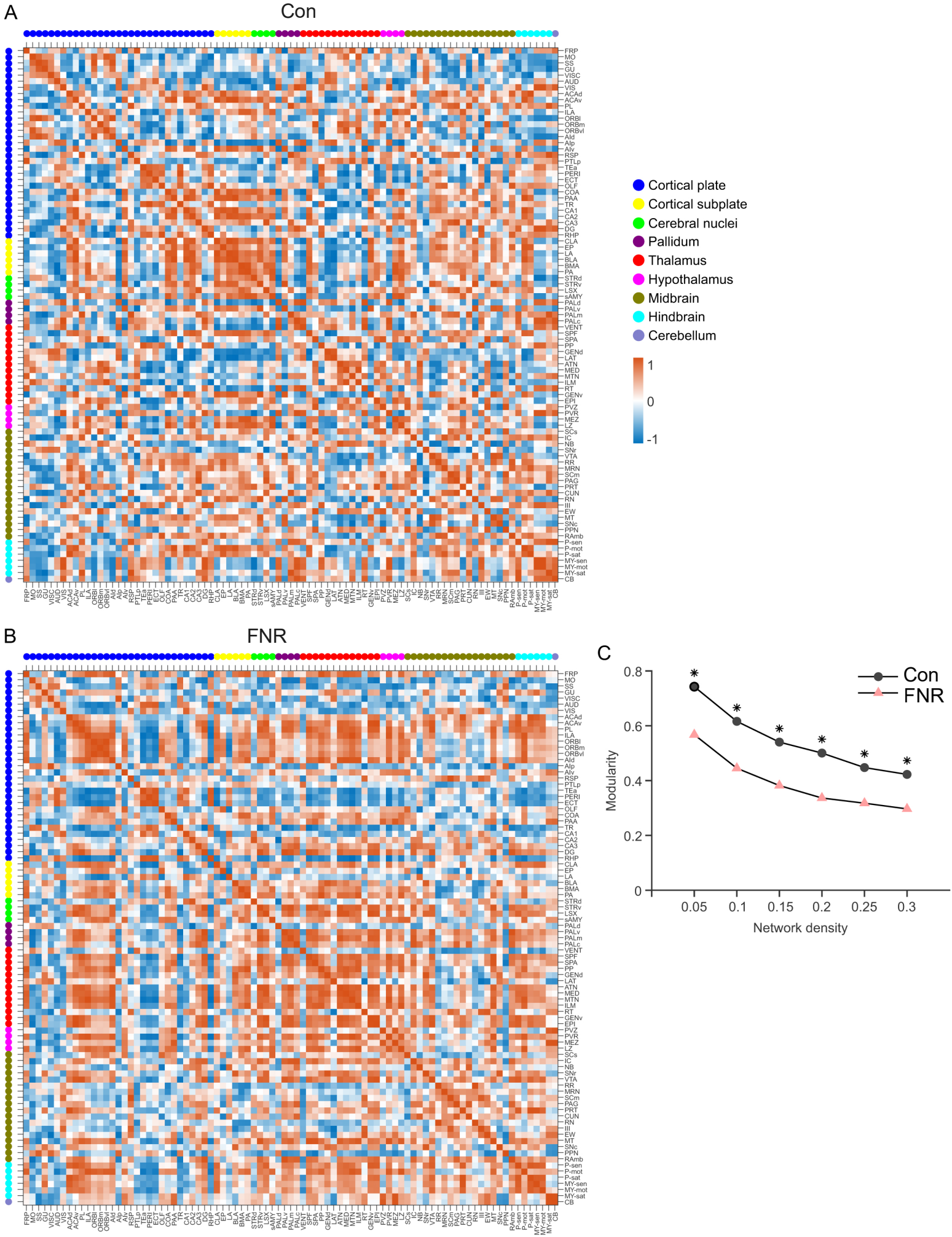
A
Con
B
FNR
C
Cortical plate
Cortical subplate
Cerebral nuclei
Pallidum
Thalamus
Hypothalamus
Midbrain
Hindbrain
Cerebellum
1
0
-1
Con
FNR
Modularity
Network density
0.8
0.6
0.4
0.2
0
0.05
0.1
0.15
0.2
0.25
0.3

Figure 8

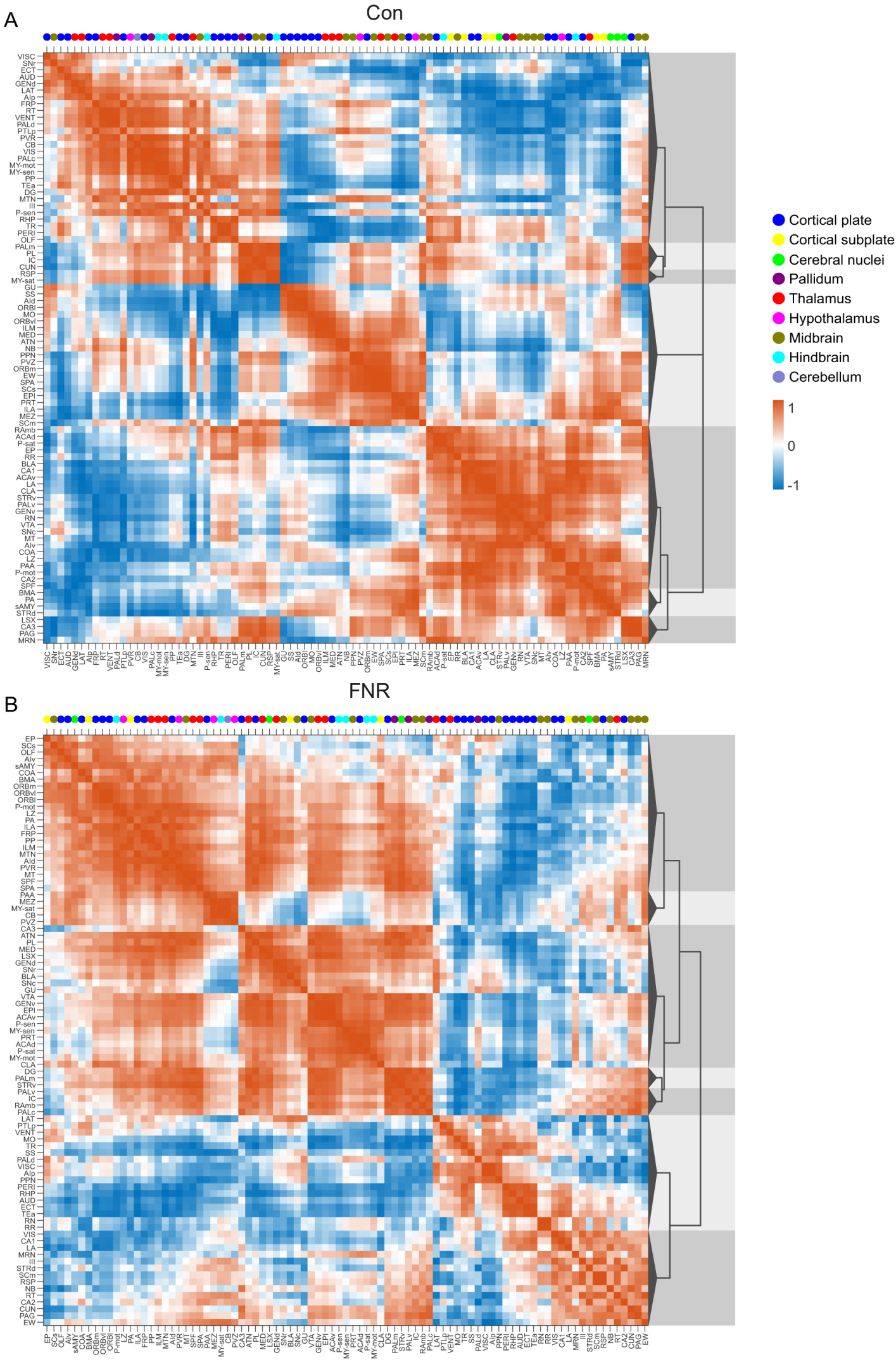
A
Con
B
FNR
Cortical plate
Cortical subplate
Cerebral nuclei
Pallidum
Thalamus
Hypothalamus
Midbrain
Hindbrain
Cerebellum
1
0
-1

Figure 9

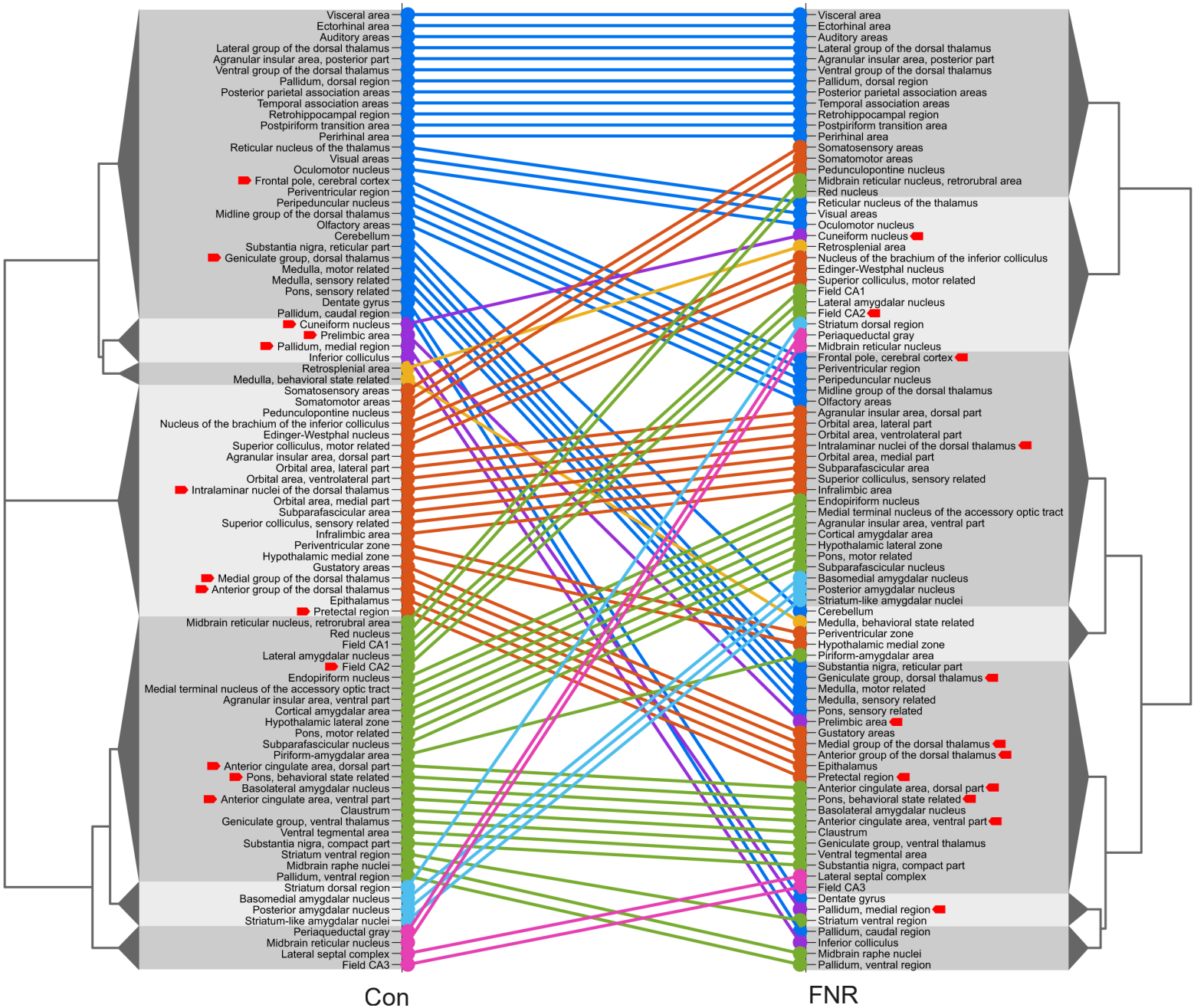
Visceral area
Ectorhinal area
Auditory areas
Lateral group of the dorsal thalamus
Agranular insular area, posterior part
Ventral group of the dorsal thalamus
Pallidum, dorsal region
Posterior parietal association areas
Temporal association areas
Retrohippocampal region
Postpiriform transition area
Perirhinal area
Reticular nucleus of the thalamus
Visual areas
Oculomotor nucleus
Frontal pole, cerebral cortex
Periventricular region
Peripeduncular nucleus
Midline group of the dorsal thalamus
Olfactory areas
Cerebellum
Substantia nigra, reticular part
Geniculate group, dorsal thalamus
Medulla, motor related
Medulla, sensory related
Pons, sensory related
Dentate gyrus
Pallidum, caudal region
Cuneiform nucleus
Prelimbic area
Pallidum, medial region
Inferior colliculus
Retrosplenial area
Medulla, behavioral state related
Somatosensory areas
Somatomotor areas
Pedunculopontine nucleus
Nucleus of the brachium of the inferior colliculus
Edinger-Westphal nucleus
Superior colliculus, motor related
Agranular insular area, dorsal part
Orbital area, lateral part
Orbital area, ventrolateral part
Intralaminar nuclei of the dorsal thalamus
Orbital area, medial part
Subparafascicular area
Superior colliculus, sensory related
Infralimbic area
Periventricular zone
Hypothalamic medial zone
Gustatory areas
Medial group of the dorsal thalamus
Anterior group of the dorsal thalamus
Epithalamus
Pretectal region
Midbrain reticular nucleus, retrorubral area
Red nucleus
Field CA1
Lateral amygdalar nucleus
Field CA2
Endopiriform nucleus
Medial terminal nucleus of the accessory optic tract
Agranular insular area, ventral part
Cortical amygdalar area
Hypothalamic lateral zone
Pons, motor related
Subparafascicular nucleus
Piriform-amygdalar area
Anterior cingulate area, dorsal part
Pons, behavioral state related
Basolateral amygdalar nucleus
Anterior cingulate area, ventral part
Claustrum
Geniculate group, ventral thalamus
Ventral tegmental area
Substantia nigra, compact part
Striatum ventral region
Midbrain raphe nuclei
Pallidum, ventral region
Striatum dorsal region
Basomedial amygdalar nucleus
Posterior amygdalar nucleus
Striatum-like amygdalar nuclei
Periaqueductal gray
Midbrain reticular nucleus
Lateral septal complex
Field CA3
Visceral area
Ectorhinal area
Auditory areas
Lateral group of the dorsal thalamus
Agranular insular area, posterior part
Ventral group of the dorsal thalamus
Pallidum, dorsal region
Posterior parietal association areas
Temporal association areas
Retrohippocampal region
Postpiriform transition area
Perirhinal area
Somatosensory areas
Somatomotor areas
Pedunculopontine nucleus
Midbrain reticular nucleus, retrorubral area
Red nucleus
Reticular nucleus of the thalamus
Visual areas
Oculomotor nucleus
Cuneiform nucleus
Retrosplenial area
Nucleus of the brachium of the inferior colliculus
Edinger-Westphal nucleus
Superior colliculus, motor related
Field CA1
Lateral amygdalar nucleus
Field CA2
Striatum dorsal region
Periaqueductal gray
Midbrain reticular nucleus
Frontal pole, cerebral cortex
Periventricular region
Peripeduncular nucleus
Midline group of the dorsal thalamus
Olfactory areas
Agranular insular area, dorsal part
Orbital area, lateral part
Orbital area, ventrolateral part
Intralaminar nuclei of the dorsal thalamus
Orbital area, medial part
Subparafascicular area
Superior colliculus, sensory related
Infralimbic area
Endopiriform nucleus
Medial terminal nucleus of the accessory optic tract
Agranular insular area, ventral part
Cortical amygdalar area
Hypothalamic lateral zone
Pons, motor related
Subparafascicular nucleus
Basomedial amygdalar nucleus
Posterior amygdalar nucleus
Striatum-like amygdalar nuclei
Cerebellum
Medulla, behavioral state related
Periventricular zone
Hypothalamic medial zone
Piriform-amygdalar area
Substantia nigra, reticular part
Geniculate group, dorsal thalamus
Medulla, motor related
Medulla, sensory related
Pons, sensory related
Prelimbic area
Gustatory areas
Medial group of the dorsal thalamus
Anterior group of the dorsal thalamus
Epithalamus
Pretectal region
Anterior cingulate area, dorsal part
Pons, behavioral state related
Basolateral amygdalar nucleus
Anterior cingulate area, ventral part
Claustrum
Geniculate group, ventral thalamus
Ventral tegmental area
Substantia nigra, compact part
Lateral septal complex
Field CA3
Dentate gyrus
Pallidum, medial region
Striatum ventral region
Pallidum, caudal region
Inferior colliculus
Midbrain raphe nuclei
Pallidum, ventral region
Con
FNR

Figure S1

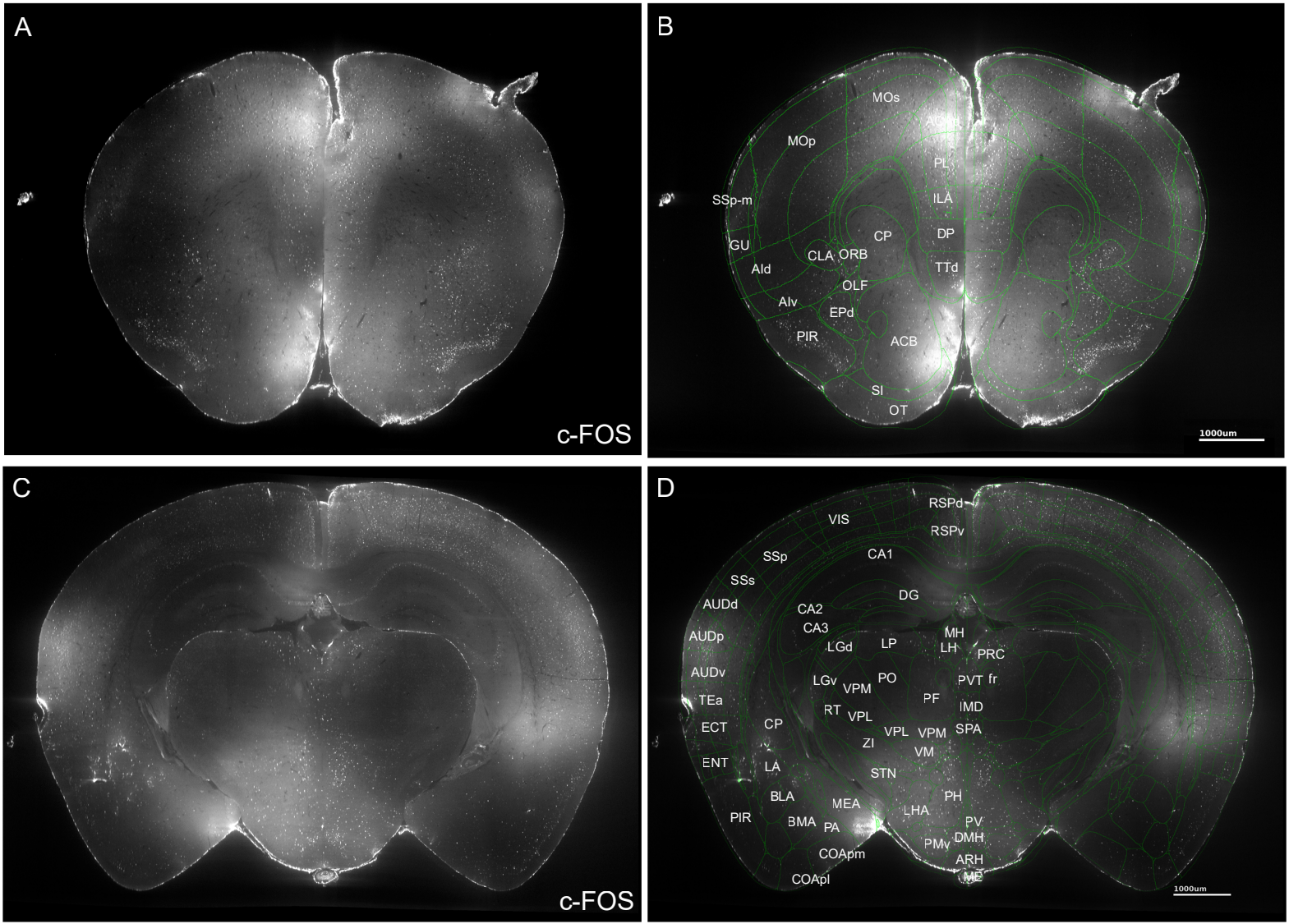
A
c-FOS
B
MOs
ACA
MOp
PL
SSp-m
ILA
CP
DP
GU
CLA
ORB
Ald
TTd
OLF
Alv
EPd
PIR
ACB
SI
OT
1000um
C
c-FOS
D
RSPd
VIS
RSPv
SSp
CA1
SSs
DG
AUDd
CA2
CA3
MH
AUDp
LGd
LP
LH
PRC
AUDv
LGv
VPM
PO
PVT
fr
TEa
PF
RT
VPL
IMD
ECT
CP
VPL
VPM
SPA
ZI
VM
ENT
LA
STN
BLA
PH
MEA
LHA
PIR
BMA
PA
PV
PMv
DMH
COApm
ARH
COApl
ME
1000um

Click here to access/download;Supplement (Word doc);Supplementary information.docx

Supplementary Information

METHODS AND MATERIALS

Animals

All animal procedures followed the US National Institutes of Health Guidelines Using Animals in Intramural Research and were approved by the National Institute of Mental Health Animal Care and Use Committee. C57BL/6J mice and BALB/c mice used in this study were bred in house using breeders purchased from The Jackson Laboratory (#000664, #000651). Mice used in behavioral experiments were maintained under a 12-hour reversed light (8 pm–8 am)/dark (8 am–8 pm) cycle with access to water and food *ad libitum* except during the APRO period when animals were given ad libitum access to water for 1 hr per day. Mice were individually housed for two days before aggression testing. For all other behavioral tests, two mice were housed in a divided cage and separated by a partition. Animals were randomly assigned to experimental groups.

APRO

Mice (35 days old; male and female) were placed under water restriction for three days during which they were given ad libitum access to water for 1 hour per day. The apparatus used for APRO was constructed by NIMH Section on Instrumentation. It is a closed running track (50L x 10W x 15H cm) with a spout installed at each end and a LED light mounted next to the spout. The mouse was allowed to run freely in the track for one 15-min session per day. The mouse could lick the spout when it reached the end of the track.

If the mouse licked the spout other than the previous one it had licked, the LED light came on for 2 sec and a water drop was delivered from the spout.

During training sessions, the mouse received water reward for every correct spout licking. Only mice making ≥12 licks on each side by Day 3 proceeded to Day 4 and 5 of APRO. On Days 4 and 5, mice run on the same track with the same rules. While control mice received water reward for all correct lickings on Days 4 and 5, water reward was delivered for only 50% of correct lickings on Day 4 and 20% on Day 5 for mice subjected to FNR. Thirty minutes after the FNR session on Day 5, the mice were subjected to a battery of behavioral tests, including the open field, resident intruder, elevated zero-maze, light/dark, forced swim, sucrose preference, and three-chamber social preference tests. Different cohorts of mice were used for each behavioral test so that each mouse was subjected to only one behavioral test. For the extinction experiment performed on Day 6, mice were run in the track for 15 minutes without light or water reward regardless of which spout they licked. All behavioral tests were conducted under red lights in the dark cycle of the animal. Behavioral data were analyzed blindly.

Behavioral testing

Open field test

Mice were allowed to freely explore an opaque box (48L x 48W x 40H cm) for 20 minutes. The behavioral data were analyzed by using ANY-maze software (Stoelting, USA) to calculate the total distance travelled, and the time spent in the center zone that accounted for 25% of the total area.

Resident Intruder Test

After the training session on Day 3, mice were housed singly in cages. Resident Intruder tests were conducted in the animal's home cage. On Day 5, mice were returned to their home cages after the FNR session. A smaller BALB/c mouse of the same sex was introduced into the cage 30 min later. The cage was covered with a transparent plexiglass lid. The two mice were allowed to interact for 5 min. If bodily injury resulted from the interaction between the resident and intruder mice, testing was discontinued, and the data were excluded from further analysis. The data from the resident intruder test were analyzed manually by a researcher blinded to experimental conditions. Based on previous studies, clinching, chasing, boxing, pinning, keeping down, and wrestling were identified as aggressive behavior (1, 2). Anogenital sniffing, grooming, inquiry, and flank rubbing were classified as nonaggressive social behaviors (3).

Elevated zero-maze test

Mice were allowed to freely explore an elevated zero-maze (blue acrylic annular platform, 105 cm in diameter and 5.5 cm wide, elevated 60 cm above the ground) for 5 minutes. The maze consisted of two closed quadrants with walls of 30-cm high and two open quadrants with no walls. ANY-maze software was used to calculate time spent, and entries to, the open quadrant.

Light/dark box test

The test box was divided into two compartments (27 L x 27 W x 30 H cm) with an opening in between to allow the mouse to enter. The light chamber had white walls and was

illuminated, while the dark compartment had black walls and was not illuminated. Mice were placed in the light box when the test started and allowed to freely explore the box for 5 min. ANY-maze software was used to calculate the percentage of time spent in the light compartment and the number of transitions between the light and dark compartments.

Forced swim test

Mice were gently released into a Plexiglas cylinder (20 H x 10 D cm) filled with water (23°C, 7.5 cm deep) and left in the water for 5 minutes. ANY-maze software was used to calculate the total immobility time, number of immobile episodes, and delay to the first immobile episode.

Three-chamber social preference test

The social preference test described by Rein et al., 2020 (4) was used with some modifications. The test has three phases: habituation, pre-testing, and testing. During habituation, the openings between the central and side chambers were blocked. There was an empty metal wire cup inside each side chamber. The mouse was placed in the central chamber and allowed to freely explore for 5 min. During the pre-test, the blocks between the central and side chambers were removed. Identical objects (blue Lego bricks) were placed in the cups. The mouse was allowed to interact freely with the objects for 5 min. After the pre-testing phase, the mouse was held temporarily in the central chamber. One object was replaced by a social stimulus (an age- and sex-matched C57BL/6 mouse) and another object was replaced by a novel object (hexagonal Lego brick). The mouse was then released to freely explore the social and non-social stimuli

for 10 min. ANY-maze software was used to record the time spent with social stimulus (mouse) and non-social stimulus (object) during the test session.

Sucrose preference test

The sucrose preference test was performed as described by Liu et al., 2018 (5), with modifications. The test has three phases: adaptation, baseline measurement, and testing after FNR. During the adaptation phase, two bottles, one containing water and the other one containing 2% sucrose solution, were inserted into the cage lid. The mouse (P29) was housed in a cage with two bottles for 2 days. The position of the bottles was switched on the second day. Both bottles were removed at 6 pm of the second day. The baseline measurement started at 9 am of the following day. Fresh bottles containing 2% sucrose and water were weighed and inserted into the cage lid. The bottles were weighed 6 hrs and 22 hrs later to determine the baseline sucrose preference index. Mice who consumed no sucrose solution during the baseline measurement period were excluded from further testing. The sucrose preference testing after FNR started 1 hr after the animal was returned to its home cage following the FNR session. Weighed water bottle and sucrose solution bottle were inserted into the cage lid. The bottles were weighed 6 hr and 22 hr later to determine the post-FNR sucrose preference index.

c-Fos imaging

Brain clearing, immunohistochemistry, light sheet microscopy, and image analysis

Mice anesthetized with isoflurane were transcardially perfused with cold phosphate buffered saline (PBS, PH 7.4) and 4% paraformaldehyde (PFA) in PBS sequentially. The

brain was removed and post-fixed in PFA for 24 hrs at 4°C, followed by rinsing in PBS three times (30 min each time) before being transferred to PBS containing 0.1% sodium azide. We employed the SHEILD method to clear the brain and eFLASH technology with stochastic electrotransport and SWITCH for immunolabeling (LifeCanvas Technologies). The brains were cleared in the delipidation buffer at 42°C for 48 hr using Smartpro Clear II (LifeCanvas Technologies, MA, USA). Cleared brains were co-incubated with the rabbit anti-c-Fos monoclonal antibody (Abcam, #ab214672) and mouse anti-NeuN monoclonal antibody (Encor Biotechnology, #MCA-1B7). After rinse, the brains were incubated with secondary antibodies in ratios of 1:2 primary:secondary molar ratio (Jackson ImmunoResearch).

After immunostaining, the brains were incubated with EasyIndex to render them transparent (RI = 1.5). The brains were then mounted in agar blocks, re-immersed in EasyIndex to match the refractive index of the brain and imaged with a SmartSPIM light sheet microscope (LifeCanvas Technologies). Images were acquired throughout the brain at 3.6X magnification, 1.8 µm/pixel resolution on the XY plane, and 4 µm thickness along the z-axis. After image acquisition, the images were tile-corrected, de-striped, and registered to the Allen Brain Atlas using an automated process (6).

A custom convolutional neural network was used for automated detection of c-Fos positive cells by Life canvas tech using the TensorFlow python package. Two networks were used: a U-Net architecture based fully-convolutional network was used for detection and a ResNet based convolutional network was used to classify a c-FOS positive or negative hit (7, 8). The c-Fos images were registered with the Allen Brain Atlas to determine the location of c-FOS positive cells. The density of c-Fos positive cells for each

brain region were calculated by dividing the total number of c-Fos positive cells in each brain region by the region volume, then averaged between the two hemispheres.

Construction of brain co-activation networks

We constructed connected, undirected, signed, weighted networks for the control and FNR groups from interregional correlations for the control and FNR groups by Pearson correlation coefficients. To calculate Pearson correlation coefficients, the density of c-Fos positive neurons in each of the 87 brain regions was multiplied by a factor to make the total number of c-Fos positive neurons in each brain equal the mean within the same treatment group (control or FNR). Pearson correlation coefficient was calculated between all pairs of the 87 brain regions within the same treatment group.

Calculation of modularity index

To compare network properties between the control and FNR groups, we calculated the modularity index Q, which quantifies the extent to which the brain exhibits a modular structure. The modularity index was calculated using the Louvain greedy algorithm (9) implemented in the Brain Connectivity Toolbox (10). We set the threshold of network density to 0.05, 0.1, 0.15, 0.2, 0.25 and 0.3. Network connections below threshold were removed. The Louvain algorithm is a heuristic to detect communities based on maximizing the modularity index. First, the algorithm combines nodes into small communities by maximizing modularity locally. Second, the small communities were used as new nodes to build a new network. This process is repeated until there is no further increase in modularity (9-11). Considering the stochastic initialization of the greedy optimization, we applied the algorithm 1000 times for each group, and used the highest

modularity index. To calculate modularity, we used vector g to denote partition of a network, where g_i denoted the cluster assignment of node i. The following modularity index formula adapted from Reichardt and Bornholdt (12) was used:

$$Q(\vec{g},\gamma) = \sum_{i,j=1}^{n} (A_{ij} - \gamma P_{ij})\delta(g_i, g_j), \quad (1)$$

where A is the connection matrix, P is the expected connection matrix under a null model, γ is the resolution parameter, and $\delta\ (g_i, g_j)$ is the community co-assignment matrix, where $\delta = 1$ if $g_i = g_j$, and $\delta = 0$ otherwise. We used the following typical null model to derive P:

$$P_{ij} = \frac{k_i k_j}{v}, \quad (2)$$

where k was the sum of all correlations of a given node, and v was the sum of all k values. We set γ to 1 for both control and FNR groups. To estimate the statistical significance of the difference in modularity index between groups, permutation tests were used by shuffling the relationship between animal ID and c-Fos positive neuron counts within each brain region. 5000 permutations were used. The permutation test results for each network density were then corrected for multiple comparisons by estimating false discovery rate (FDR) with Benjamini–Hochberg procedure.

Hierarchical Consensus clustering

Hierarchical consensus clustering was done using a pipeline developed by Jeub et al. (13). We used the correlation matrices without thresholding for consensus clustering, a procedure which combines multiple partitions for the same network to obtain a consensus partition for the network. Consensus clustering was started by multiresolution clustering, conducted by sampling the γ value 1000 times between [γ_{min}, γ_{max}] to obtain a series of

partitions with different resolutions. γ_{max} was the smallest value of γ such that $A_{ij} - \gamma P_{ij} \leq 0$ for all *i* and *j*. γ_{min} was the max value of γ when a given partition was the trivial partition where all nodes were in the same community. We generated a co-classification matrix *C*, defined as the probability that two nodes were assigned to the same community, from the 1000 partitions corresponding to the sampled *γ* values.

Matrix *C* was used to obtain a new ensemble of partitions by optimizing equation (3) using iterated GenLouvain (13, 14)

$$Q_C(\vec{g}, \alpha) = \sum \left(C_{ij} - P_{ij}^{null}(\alpha) \right) \delta(g_i, g_j), \tag{3}$$

where *α* was the significance level, and $P_{ij}^{null}(\alpha)$ was the highest value between the expected probability of *i* belonging to the same community of *j* and vice-versa in a local permutation model. *α* was set at 0.001. We then computed a new co-classification matrix for the new ensemble and repeated the procedure until the co-classification matrix is binary to obtain a consensus clustering as suggested by Lancichinetti and Fortunato (15).

The consensus clustering was used to generate a hierarchical cluster tree with recursive strategy. We applied consensus clustering as described above to a partition where all nodes were in the same community. Then we repeated the procedure for each newly generated community and restricted it to the nodes within each community. This procedure stopped once there were no more communities that could be further split into sub-communities at the given significance level.

Data and statistical analysis:

Graphpad prism (9.5.1) was utilized for statistical analysis. For behavioral analysis, two-tailed Student's t-test was used for normally distributed data with equal variance and Mann-Whitney U test was used for data that did not satisfy these requirements. One-way ANOVA on ranks or two-way ANOVA with Dunn's procedures or Tukey's test for post hoc multiple comparisons were used for comparing more than two groups. The density of c-Fos positive neurons was analyzed with two-tailed Student's t-test to compare between control and FNR mice and the obtained p-values were adjusted with the FDR approach. $P < 0.05$ was considered significant. All data are presented as the mean + SEM. Statistical results for all figures are provided in Table S1.

References

1. Koolhaas JM, Coppens CM, de Boer SF, Buwalda B, Meerlo P, Timmermans PJ (2013): The resident-intruder paradigm: a standardized test for aggression, violence and social stress. *J Vis Exp*.e4367.

2. Nelson RJ, Trainor BC (2007): Neural mechanisms of aggression. *Nat Rev Neurosci*. 8:536-546.

3. Nordman J, Ma X, Li Z (2020): Traumatic Stress Induces Prolonged Aggression Increase through Synaptic Potentiation in the Medial Amygdala Circuits. *eNeuro*. 7.

4. Rein B, Ma K, Yan Z (2020): A standardized social preference protocol for measuring social deficits in mouse models of autism. *Nat Protoc*. 15:3464-3477.

5. Liu MY, Yin CY, Zhu LJ, Zhu XH, Xu C, Luo CX, et al. (2018): Sucrose preference test for measurement of stress-induced anhedonia in mice. *Nat Protoc*. 13:1686-1698.

6. Marstal K, Berendsen F, Staring M, Klein S (2016): SimpleElastix: A user-friendly, multi-lingual library for medical image registration. *Ieee Comput Soc Conf*.574-582.

7. Shelhamer E, Long J, Darrell T (2017): Fully Convolutional Networks for Semantic Segmentation. *IEEE Trans Pattern Anal Mach Intell*. 39:640-651.

8. Ronneberger O, Fischer P, Brox T (2015): U-Net: Convolutional Networks for Biomedical Image Segmentation. *Medical Image Computing and Computer-Assisted Intervention, Pt Iii*. 9351:234-241.

9. Blondel VD, Guillaume JL, Lambiotte R, Lefebvre E (2008): Fast unfolding of communities in large networks. *J Stat Mech-Theory E*.

10. Rubinov M, Sporns O (2010): Complex network measures of brain connectivity: uses and interpretations. *Neuroimage*. 52:1059-1069.

11. Newman ME (2006): Modularity and community structure in networks. *Proc Natl Acad Sci U S A*. 103:8577-8582.

12. Reichardt J, Bornholdt S (2006): Statistical mechanics of community detection. *Phys Rev E Stat Nonlin Soft Matter Phys*. 74:016110.

13. Jeub LGS, Sporns O, Fortunato S (2018): Multiresolution Consensus Clustering in Networks. *Sci Rep*. 8:3259.

14. Jeub LGS, Bazzi, M., Jutla, I. S. & Mucha, P. J. ((2011–2016)): GenLouvain 2.1: A generalized Louvain method for community
detection implemented in MATLAB.

15. Lancichinetti A, Fortunato S (2012): Consensus clustering in complex networks. *Sci Rep*. 2:336.